THE JOURNAL OF PHYSICAL CHEMISTRY C

Article

pubs.acs.org/JPCC

Growth, Structure, and Anisotropic Optical Properties of Difluoro-anthradithiophene Thin Films

Timo Storzer,[†] Alexander Hinderhofer,*[,†] Clemens Zeiser,[†] Jiří Novák,[‡] Zbyněk Fišer,[‡] Valentina Belova,[†] Berthold Reisz,[†] Santanu Maiti,[†] Giuliano Duva,[†] Rawad K. Hallani,[§] Alexander Gerlach,[†] John E. Anthony,[§] and Frank Schreiber[†]

[†]Institute for Applied Physics, University of Tübingen, Auf der Morgenstelle 10, 72076 Tübingen, Germany

[‡]CEITEC, Masaryk University and Department of Condensed Matter Physics, Faculty of Science, Masaryk University, Kotlářská 2, CZ-611 37 Brno, Czech Republic

[§]Department of Chemistry, University of Kentucky, Lexington, Kentucky 40506-0055, United States

S *Supporting Information*

ABSTRACT: Anthradithiophene (ADT) and its functionalized derivatives have proven to be attractive for high-performance electronic devices based on small-molecule organic semiconductors. In this manuscript we investigate the structural and optical properties of thin films of difluoro-anthradithiophene (diF-ADT), an ADT derivative, grown by organic molecular beam deposition (OMBD). By grazing incidence X-ray diffraction and reciprocal space maps, we show that diF-ADT crystallizes in a thin film structure similar to the single crystal unit cell. In addition, we investigate the growth characteristics with atomic force microscopy (AFM) and show an increase of surface mound sizes with elevated substrate temperature. Optical absorption measurements reveal a clear vibronic progression in both solution and thin film spectra along with a distinct optical anisotropy related to the molecular orientation in thin films.

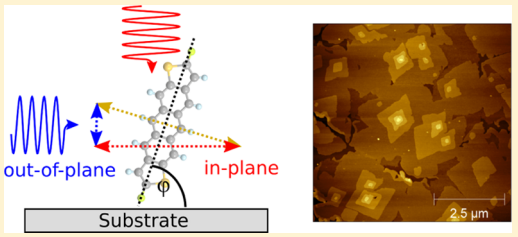

I. INTRODUCTION

Thin films based on small-molecule organic semiconductors continue to attract attention as key building blocks of optoelectronic devices, among them organic light-emitting diodes (OLEDs), organic field-effect transistors (OFETs) and organic photovoltaics (OPV). Their ease of processability and chemical tunability makes them predestined for application in disposable and inexpensive large-area electronics.[1−9]

In organic crystals, typically the transfer integrals coupling molecules are smaller in comparison to inorganic solids, which results in relatively small charge carrier mobilities.[10] However, there have been reports of charge-carrier mobilites as high as 1−10 $cm^2\ V^{-1}\ s^{-1}$, which allows organic materials to compete with amorphous silicon.[11−16] In order to achieve such a high performance in large-area devices organic materials, understanding and control of the thin film growth process is of crucial importance.[17−27]

Anthradithiophene (ADT) and its functionalized derivatives have proven to be attractive for high-performance electronic devices.[28−33] In particular the functionalization by partial fluorination exhibited accelerated crystallization and improved stability toward photooxidation.[34−36] For solution processability, side groups can be attached to anthradithiophene backbones. Among the most studied soluble ADT derivatives are TES-ADT and diF-TES-ADT, which show enhanced charge transport properties.[12,35,37−39]

Among the many preparation methods available for thin film preparation, two main methods are typically used: thermal deposition in vacuum and deposition from solution. Not all compounds can be equally well deposited with both methods. Deposition from solution requires relatively high solubility of the compound, for which solubility-enhancing side groups can be attached. On the other hand for thermal deposition the compound has to be thermally stable. Although both deposition methods have their advantages and peculiarities, deposition from vacuum usually allows for better control of the deposition process by balancing the deposition rate with the thermal diffusion on the substrate.

For vacuum-deposited organic thin films there is an increasing number of studies with a quantitative analysis of growth processes.[18,40−42] These studies are based on a theoretical description of growth mechanisms of atomic systems using a set of scaling exponents which relates the surface roughness and the lateral length scales to the film thickness[43−46] and which greatly improved the understanding of growth processes in general.

This paper is dedicated to the structural and optical characterization of difluoro-anthradithiophene (diF-ADT), an ADT derivative with promising characteristics for optoelec-

Received: July 7, 2017
Revised: August 28, 2017
Published: August 30, 2017

DOI: 10.1021/acs.jpcc.7b06558
J. Phys. Chem. C 2017, 121, 21011−21017

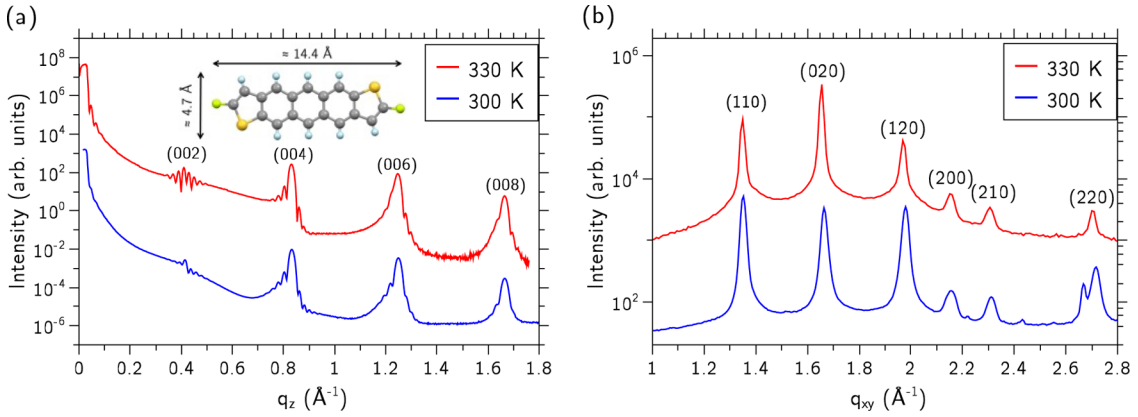

Figure 1. (a) XRR and (b) GIXD scans of 30 nm diF-ADT films grown at 300 and 330 K substrate temperature on a silicon substrate covered with a native oxide layer. Angle of incidence for GIXD was $\alpha = 0.12°$ ($\lambda = 0.103$ nm).

tronic applications. It is organized as follows: Section III.A presents X-ray scattering data providing information on the structure of diF-ADT in thin films. In Section III.B surface morphology images and the height−height correlation of films of increasing thickness are analyzed by scaling laws. Optical absorption spectra comparing monomers in solution to condensed thin films are presented in Section III.C.

II. EXPERIMENTAL SECTION

Thin films of diF-ADT were grown in an organic molecular beam deposition (OMBD)[47−49] chamber under high vacuum conditions (base pressure = 2×10^{-8} mbar). Prior to film growth the silicon substrates (Si(100) wafers covered with a native oxide layer) and glass substrates were cleaned in an ultrasonic bath with acetone and isopropyl alcohol and afterward heated to 500 K for degassing. During film growth the substrate temperature was either kept at 300 or 330 K. The growth rates were 0.5 and 3.0 Å/min monitored with an SQM-160 quartz crystal microbalance (Inficon, Switzerland).

After film growth surface morphology images were obtained by atomic force microscopy (AFM) using a NanoWizard II (JPK Instruments, Germany) in tapping mode. X-ray reflectivity (XRR), grazing incidence X-ray diffraction (GIXD) and reciprocal space maps were done either at beamline ID10 (ESRF, France) or at the X04SA beamline (SLS, Switzerland). All X-ray scattering experiments were performed under vacuum.

Optical absorption in the UV−vis range was measured with a Cary 50 spectrophotometer (Varian Inc., USA) on glass substrates under normal incidence. Thin films on both silicon and glass substrates were used for variable angle spectroscopic ellipsometry (VASE) measurements using an M-2000 ellipsometer (J.A. Woollam Co., USA).

III. RESULTS AND DISCUSSION

III.A. X-ray Scattering. High-resolution X-ray scattering experiments were performed in order to determine the crystal structure of diF-ADT in thin films. XRR (Figure 1a) and GIXD (Figure 1b) data provide information on the out-of-plane lattice spacing and the in-plane structure, respectively. In Figure 1 we observe pronounced Bragg reflections in both the in-plane and in the out-of-plane direction showing that diF-ADT thin films are highly crystalline. From the position of the Bragg reflection series in XRR we derive an out-of-plane lattice spacing of d_{00l} = 1.51 nm. This length is not too different from the length of the long axis of the diF-ADT molecule, which is 1.44 nm, suggesting that the molecules grow in a standing-up configuration on silicon substrates.

The small intensity of the (002) Bragg peak is likely induced by the unusual electron density ρ distribution of the diF-ADT molecule, where ρ is larger at the ends of the molecule than in the center. The asymmetry of the higher order Bragg reflections indicates that there might be slightly different lattice plane spacings for the molecular layers near the substrate associated with slightly different molecular tilt angles. This may cause interference effects that result in the uncommon shape of the first Bragg reflection.

In order to quantify the unit cell parameters, a reciprocal space map of a diF-ADT film was recorded (Figure 2). The

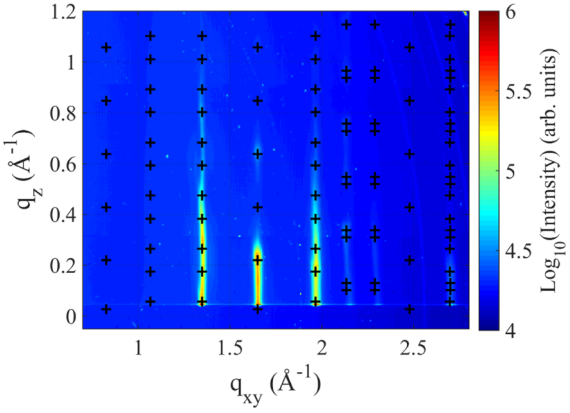

Figure 2. Reciprocal space map of a 50 nm diF-ADT thin film grown at 330 K on a silicon substrate covered with a native oxide layer. The q-map is assembled from 36 single pictures that were taken with a Pilatus 300k area detector. Calculated Bragg peak positions from the unit cell in Table 1 are indicated by black crosses.

three pronounced rod-like reflections can be assigned to the (11l), (02l) and (12l) directions. To determine the thin film unit cell we used the single crystal unit cell parameters as starting point and adjusted them iteratively in order to obtain the best fit to the reflections in Figure 2. The calculated peak positions were corrected for the refractive index of the thin film.[50] The unit cell parameters with the best match to the experimental data are shown in Table 1 together with the unit cell parameters from the single crystal. All unit cell lengths are slightly increased, where the relative increase is strongest in the

DOI: 10.1021/acs.jpcc.7b06558
J. Phys. Chem. C 2017, 121, 21011−21017

Table 1. Comparison of the Unit Cell Parameters of the Single Crystal (SC) and the Thin Film

	a (Å)	b (Å)	c (Å)	α (deg)	β (deg)	γ (deg)	vol (Å^3)
SC (90 K)[53]	5.8573	7.4715	29.9378	90	91.878	90	1309.46
thin film (300 K)	5.89	7.61	30.04	90	92.4	90	1345.5

b-axis. Furthermore, the monoclinic angle β is increased by about 0.55°. Correspondingly, the unit cell volume is increased. We note that the single crystal and thin film unit cells were determined at different T (90 and 300 K), which might partially explain the observed differences. However, the resulting volumetric thermal expansion coefficient of $\alpha_V = 130 \times 10^{-6}$ K^{-1} would be much higher than for comparable compounds,[51] if the unit cell change was a pure temperature effect.

We note that the fitting of unit cell parameters from thin film data has several peculiarities related to the low intensity and large width of the reflections. This makes an unambiguous determination of the unit cell somewhat difficult. Because of the large peak width, for example, the fitting process is not very sensitive to small deviations in unit cell angles α and γ, i.e., it is also possible to fit this q-map using a triclinic unit cell with angles close to 90°. Nevertheless, while determination of the structure is not absolute, the deviations from the single crystal unit cell are sufficient to conclude that there is likely a surface-induced thin film polymorph.[52]

In contrast to other organic semiconductors, where the thin film polymorph frequently shows a clear elongation of the unit cell in the direction perpendicular to the surface plane with more upright oriented molecules, for example as in pentacene,[52] we do not find a strong elongation of the c-axis for diF-ADT. This may be due to the strong F−H intermolecular hydrogen bonding in the diF-ADT structure, which enhances interactions between molecules along the c-axis.

In addition to the crystal structure determination, we determined the coherent in-plane island size of dif-ADT-dependent on the temperature from GIXD data (Figure 1b). Using the full width at half-maximum (fwhm) of the Bragg reflections we determined the coherently scattering in-plane domain size from the Scherrer formula via $D_{coh\|} = 2\pi \cdot 0.94/\text{fwhm}$. The values of $D_{coh\|}$ in Table 2 are averaged values of the (110), (020), and (120) reflections.

Table 2. Averaged Coherently Scattering Domain Size $D_{coh\|}$ of the (110), (020), and (120) Reflections[a]

T_{sub} (K)	$D_{coh\|}$ (nm)
300	26.2 ± 2.5
330	33.0 ± 4.1

[a] $D_{coh\|}$ increases with increasing substrate temperature.

At elevated temperature we observe a slight increase of $D_{coh\|}$, which is consistent with the conventional expectation that with higher T the nucleation density decreases due to the higher diffusion length of the molecules.

III.B. Atomic Force Microscopy. In order to study the influence of the substrate temperature on the surface morphology of diF-ADT thin films, two sample series were prepared. Each series for temperatures 300 and 330 K, respectively, consists of samples with nominal film thickness ranging from 4 to 50 nm. The deposition rate was kept constant at 0.5 Å/min (4 nm) and at 3 Å/min (10, 30, and 50 nm), respectively.

Figure 3 shows representative AFM scans of the films. An increase of the film thickness leads to an increase of the domain size in both the high and low temperature series grown at 3 Å/min. We note that the 4 nm thin films were grown at a substantially lower growth rate resulting in larger lateral domains. A direct comparison of films with the same thickness, but grown at different substrate temperatures, reveals that even at a temperature elevated by only 30 K the mound size is considerably larger. The 50 nm film at high temperature exhibits terraced mounds of pyramidal shape, signifying that there is preferential growth along certain crystallographic directions. The step height of the terraces is approximately 1.5 nm, which is consistent with the lattice spacing determined by XRR, i.e., the steps are monomolecular.

A quantitative analysis of the height−height correlation functions (HHCF) of the AFM images can provide insight into the growth mode[44] of diF-ADT. For each sample the HHCFs of several AFM scans were fitted by the function $f(x) = 2\sigma^2[1 - \exp(-(x/\xi)^2)]$. The resulting lateral correlation coefficients ξ, which are a measure for the surface domain size, were averaged to obtain statistically relevant information (Figure 4a). In order to achieve an accurate evaluation of the root-mean-squared roughness σ, σ_{AFM} extracted from the HHCF were averaged with the respective values σ_{XRR} obtained from X-ray reflectivity, which provides a large-area averaged roughness value for each sample.

We note that the HHCF of the 50 nm (300 K) film, which exhibits a rather broad distribution of island sizes (see AFM data in Figure 3d), does not reveal a clearly defined point where the linear part of the HHCF turns into the saturation part. This might be an indication that under these specific growth conditions not only one simple growth scenario dominates.

Within the dynamic scaling framework[54] one expects a power-law dependence relating the lateral correlation length ξ and the film thickness D with $\xi \sim D^{1/z}$. The dynamic exponent $1/z$ is a measure for the thickness dependent increase of the correlation length ξ, or in simplified view describes how fast separate islands are coalescing. A linear regression to the plotted data points on a log−log scale is shown in Figure 4a.

For the 300 K samples $1/z(T_{sub}^{300K}) = 0.70 \pm 0.16$ is similar to that of the organic semiconductor diindenoperylene (DIP, $1/z = 0.92 \pm 0.20$), which exhibits a rapid roughening behavior with fast island coalescing.[40] By contrast, at 330 K ξ does not change substantially with film thickness with $1/z(T_{sub}^{330K}) = 0.14 \pm 0.20$. To put these values into perspective, we should expect $1/z \approx 0.25$ for samples with wedding-cake-shaped growth morphology generated by high step edge barriers.[44]

Analogous to the correlation length, the power-law dependence of the root mean square (rms)-roughness on the film thickness, $\sigma \sim D^{\beta}$, can be analyzed with a linear fit of the data on a log−log scale (Figure 4b). For both substrate temperatures we find a nearly identical growth exponent of $\beta\,(T_{sub}^{300K}) = 0.53 \pm 0.17$ and $\beta\,(T_{sub}^{330K}) = 0.52 \pm 0.08$. A growth exponent of $\beta = 0.5$ would imply a terrace-like growth mode in which the mound profiles follow a Poisson distribution. Their standard deviation is given by the square root of the film thickness D ($\sigma \sim D^{1/2}$).[46,55]

DOI: 10.1021/acs.jpcc.7b06558
J. Phys. Chem. C 2017, 121, 21011−21017

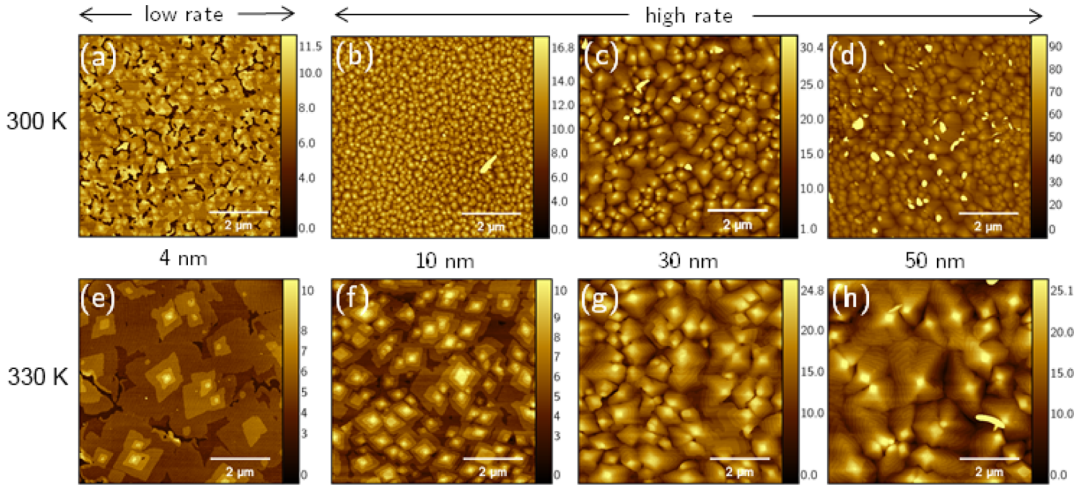

Figure 3. AFM images (image size: 7 × 7 μm^2) of films with different thickness. The substrate temperatures during growth were 300 K (a–d) and 330 K (e–h). The 4 nm films were grown at a low rate of 0.5 Å/min. The growth rate of all other samples was at a high rate of 3 Å/min. The height scale is in nm.

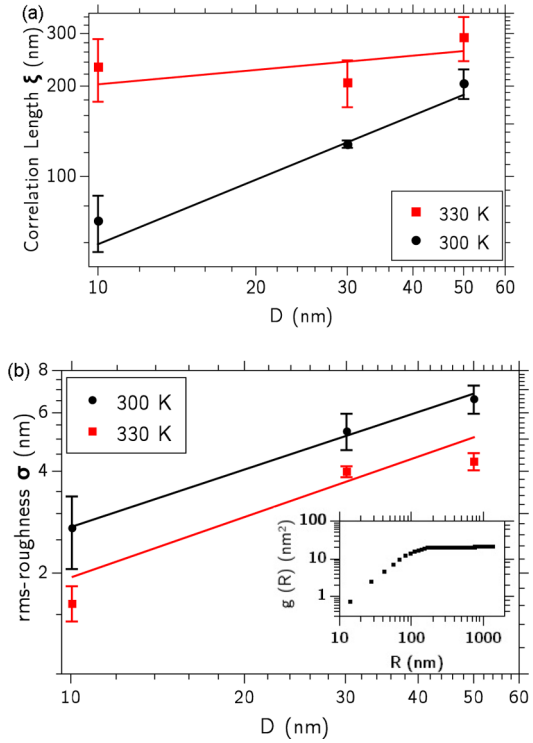

Figure 4. (a) Lateral correlation length ξ extracted from the height–height correlation function (HHCF) of AFM morphology images. (b) Averaged values of the rms-roughness extracted from the HHCF and obtained by fitting the respective XRR scans ($\sigma = (\sigma_{AFM} + \sigma_{XRR})/2$). The inset in panel b shows a typical HHCF. Data points in both images are shown for substrate temperatures 300 K (black circles) and 330 K (red squares). The straight lines through the respective data sets are linear regressions used to obtain the scaling coefficients $1/z$ and β in panels a and b, respectively.

We can put our results into a broader context by a comparison with other commonly used rod-like organic molecules. For *para*-sexiphenyl (6P), which also grows in terraced mounds, a growth exponent of $\beta = 0.49$ was found[55] and similarly for iron phthalocyanine (FePc) $\beta = 0.51 \pm 0.14$.[56]

Very different growth exponents were found for DIP[40,57] ($\beta = 0.748 \pm 0.05$ and $\beta = 0.772 \pm 0.031$), with faster roughness evolution which can be termed as unusually rapid. Other compounds, like pentacene[58] ($\beta = 0.27 \pm 0.03$) or TiOPc[59] ($\beta = 0.27 \pm 0.04$), have a much slower roughness evolution.

For technical reasons, the thickness range of this analysis is limited. At much higher thicknesses the roughness evolution behavior might change. Nevertheless the data provide a good estimate of the roughness evolution in a commonly used and application-relevant thickness range. At this point it is important to note that, for rod-like organic molecules, there might be nontrivial extensions of the scaling laws which go far beyond the relations applied.[18,40,60] Nevertheless an application of the well-established scaling laws on this new compound can be helpful for at least a coarse categorization of the growth dynamics of diF-ADT.

III.C. Optical Properties. Optical absorption spectra were obtained by UV–vis and spectroscopic ellipsometry. We find that for the present films the absorption behavior does not strongly depend on the growth parameters, such as the substrate temperature or the deposition rate. Figure 5a shows a representative absorption spectrum of a 30 nm diF-ADT film grown on a glass substrate at 300 K and for comparison the spectrum of diF-ADT dissolved in 1,2-dichlorobenzene. The solution spectrum shows a pronounced vibronic progression with the 0–0 and 0–1 transitions of similar intensity. A mean peak distance of (0.17 ± 0.01) eV corresponds to the typical spacing of vibronic excitations in aromatic compounds.

In contrast to the solution spectrum, where we observe the absorption of diF-ADT monomers with random orientation, in thin films diF-ADT is ordered in a crystalline structure with a preferred out-of-plane alignment (so-called *fiber-texture*). We observe an overall red-shift of about 0.22 eV of the whole spectrum. There is still a pronounced vibronic progression in the crystalline thin film with distinct peaks arising from the 0–0, 0–1, and 0–2 transitions. An estimation of the mean distance of the peaks yields (0.19 ± 0.01) eV. The width of all peaks is slightly increased, and the 0–0 transition exhibits a pronounced peak splitting. This splitting of an excited state into two Davydov components can occur if there are two or more molecules per unit cell,[61] which is the case for diF-ADT.

Due to their fiber-texture, diF-ADT thin films exhibit optical uniaxial anisotropy. The tilt angle φ of the molecular plane relative to the substrate determines the optical properties of the

DOI: 10.1021/acs.jpcc.7b06558
J. Phys. Chem. C 2017, 121, 21011–21017

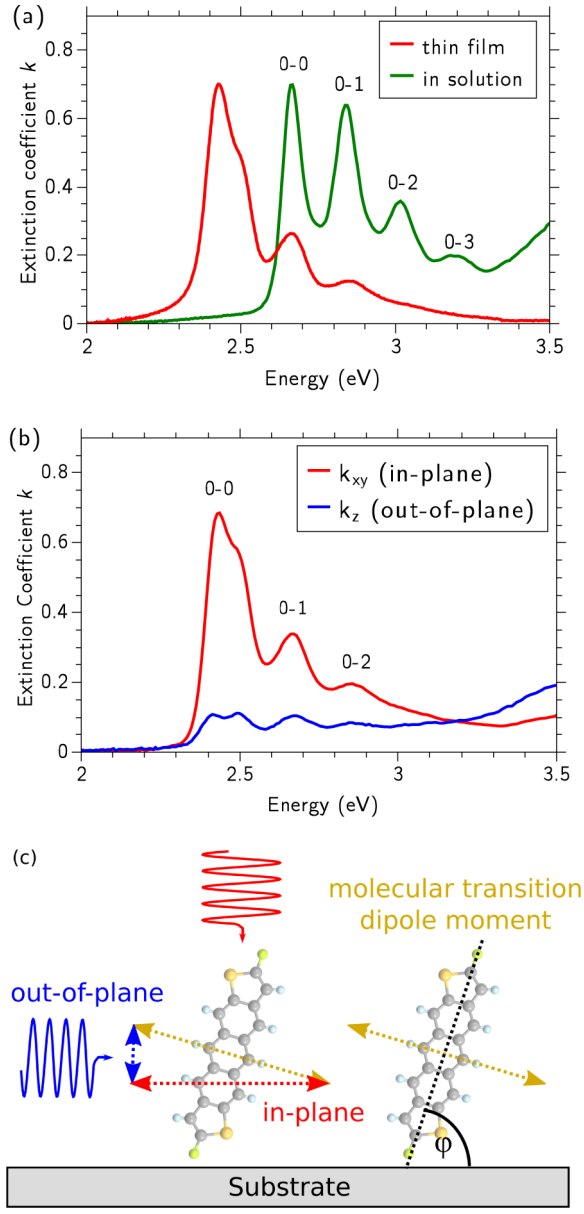

Figure 5. Extinction coefficient k determined by (a) UV−vis spectroscopy of the thin film and dissolved in dichlorobenzene and by (b) variable angle spectroscopic ellipsometry of the thin film. The intensity of the solution spectrum was normalized to the maximum value in the thin film. (c) Sketch of the orientation of the HOMO−LUMO transition dipole moment. Molecular planes are inclined by angle φ relative to the surface, which results in an optical in-plane component absorbing light impinging perpendicular to the film surface and an out-of-plane component absorbing light impinging parallel to the film surface.

in-plane component and the out-of-plane component. Since diF-ADT grows in a nearly standing-up orientation, the absorption we observe in UV−vis spectroscopy under normal incidence is predominantly caused by the transition dipole moment of the HOMO−LUMO transition, which is directed along the short axis of the molecule (Figure 5c).

By combining variable angle spectroscopic ellipsometry (VASE) in reflection mode (on silicon substrates) with transmission ellipsometry (on glass substrates), we obtain information on both the in-plane and out-of-plane component of the dielectric function. In this way we can unambiguously resolve the optical anisotropy.[62,63]

Figure 5b shows the anisotropic extinction coefficient of a thin diF-ADT film analyzed with a multisample analysis. As expected, the in-plane component k_{xy} is nearly identical to the UV−vis absorption spectrum. The intensity of the out-of-plane component k_z is very weak, confirming the nearly upright orientation of the diF-ADT molecules on the substrate. An estimation of the tilt angle from the intensity difference of the 0−0 transition in both components yields $\varphi \approx 82°$, i.e., 8° off the surface normal. This tilt angle is consistent with the thin film unit cell determined above.

CONCLUSION AND SUMMARY

We have studied the growth, structure and morphology of thin films of diF-ADT dependent on the substrate temperature. We found that diF-ADT thin films are highly crystalline and nucleate in a thin film polymorph similar to the single crystal structure. GIXD measurements have shown that the in-plane coherently scattering domain size increases at an elevated substrate temperature, which may be beneficial for transistor preparation.

From the analysis of AFM data we identified a strong dependence of the in-plane lateral correlation length on the substrate temperature. Upon an elevation of temperature by 30 K the mound size is significantly increased. The well-established concept of dynamic scaling and the analysis of scaling exponents was applied to the morphology data.

In the examined thickness range, the surface roughness evolution with increasing film thickness obeys the same scaling law with a scaling exponent of $\beta \approx 0.5$ for both substrate temperatures 300 and 330 K, but the absolute roughness value is decreased at higher temperature. In particular, we observe a growth mode which results in large *wedding-cake* islands with clearly visible terraces. This upward growth mechanism is due to the presence of a sufficiently large step edge barrier that prevents deposited molecules from hopping down to adjacent lower layers. This growth mode is likely enhanced due to the strong end-to-end attraction between these molecules from intermolecular F−H hydrogen bonding interactions as seen in the solubilized version of diF-ADT.[64]

Consistent with X-ray scattering results, we observe a characteristic shift of the HOMO−LUMO transition between the solution and thin film spectrum, where the latter exhibit a pronounced optical anisotropy. In the studied parameter range, the optical absorption measurements did not reveal a strong dependence on growth conditions.

ASSOCIATED CONTENT

Supporting Information

The Supporting Information is available free of charge on the ACS Publications website at DOI: 10.1021/acs.jpcc.7b06558.

XRR data of diF-ADT during annealing at different temperatures (PDF)

AUTHOR INFORMATION

Corresponding Author

*E-mail: alexander.hinderhofer@uni-tuebingen.de.

ORCID

Alexander Hinderhofer: 0000-0001-8152-6386

Valentina Belova: 0000-0002-8142-2090

DOI: 10.1021/acs.jpcc.7b06558
J. Phys. Chem. C 2017, 121, 21011−21017

John E. Anthony: 0000-0002-8972-1888

Notes

The authors declare no competing financial interest.

■ ACKNOWLEDGMENTS

Support from the DFG is gratefully acknowledged. G.D. acknowledges support from the Carl Zeiss foundation. J.N. acknowledges support from the project CEITEC 2020 (Grant No. LQ1601 financed by the MEYS of the Czech Republic) and CEITEC Nano Research Infrastructure (LM2015041, MEYS CR, 2016-2019). We also acknowledge support from DAAD/AWTR/MEYS Grant No. 57215815/7AMB16DE006.

■ REFERENCES

(1) Forrest, S. R. Ultrathin organic films grown by organic molecular beam deposition and related techniques. *Chem. Rev.* **1997**, *97*, 1793−1896.
(2) Forrest, S. R. The path to ubiquitous and low-cost organic electronic appliances on plastic. *Nature* **2004**, *428*, 911−918.
(3) Brabec, C.; Dyakonov, V.; Parisi, J.; Sariciftci, N. *Organic Photovoltaics: Concepts and applications*; Springer: Berlin, Heidelberg, 2003.
(4) Peumans, P.; Yakimov, A.; Forrest, S. R. Small molecular weight organic thin-film photodetectors and solar cells. *J. Appl. Phys.* **2003**, *93*, 3693−3723.
(5) Lin, Y.; Li, Y.; Zhan, X. Small molecule semiconductors for high-efficiency organic photovoltaics. *Chem. Soc. Rev.* **2012**, *41*, 4245.
(6) Reineke, S.; Lindner, F.; Schwartz, G.; Seidler, N.; Walzer, K.; Lussem, B.; Leo, K. White organic light-emitting diodes with fluorescent tube efficiency. *Nature* **2009**, *459*, 234−238.
(7) Sirringhaus, H. 25th Anniversary Article: Organic Field-Effect Transistors: The Path Beyond Amorphous Silicon. *Adv. Mater.* **2014**, *26*, 1319−1335.
(8) Katz, H. E.; Huang, J. Thin-Film Organic Electronic Devices. *Annu. Rev. Mater. Res.* **2009**, *39*, 71−92.
(9) Jou, J.-H.; Kumar, S.; Agrawal, A.; Li, T.-H.; Sahoo, S. Approaches for fabricating high efficiency organic light emitting diodes. *J. Mater. Chem. C* **2015**, *3*, 2974−3002.
(10) Schwoerer, M.; Wolf, H. C. *Organic Molecular Solids*; Wiley-VCH Verlag GmbH & Co.: Weinheim, Germany, 2005; pp XI, 427 S.
(11) Minemawari, H.; Yamada, T.; Matsui, H.; Tsutsumi, J.; Haas, S.; Chiba, R.; Kumai, R.; Hasegawa, T. Inkjet printing of single-crystal films. *Nature* **2011**, *475*, 364−367.
(12) Niazi, M. R.; Li, R.; Qiang Li, E.; Kirmani, A. R.; Abdelsamie, M.; Wang, Q.; Pan, W.; Payne, M. M.; Anthony, J. E.; Smilgies, D.-M.; et al. Solution-printed organic semiconductor blends exhibiting transport properties on par with single crystals. *Nat. Commun.* **2015**, *6*, 8598.
(13) Gundlach, D. J.; Royer, J. E.; Park, S. K.; Subramanian, S.; Jurchescu, O. D.; Hamadani, B. H.; Moad, A. J.; Kline, R. J.; Teague, L. C.; Kirillov, O.; et al. Contact-induced crystallinity for high-performance soluble acene-based transistors and circuits. *Nat. Mater.* **2008**, *7*, 216−221.
(14) Lehnherr, D.; Waterloo, A. R.; Goetz, K. P.; Payne, M. M.; Hampel, F.; Anthony, J. E.; Jurchescu, O. D.; Tykwinski, R. R. Isomerically Pure syn-Anthradithiophenes: Synthesis, Properties, and FET Performance. *Org. Lett.* **2012**, *14*, 3660−3663.
(15) Shinamura, S.; Osaka, I.; Miyazaki, E.; Nakao, A.; Yamagishi, M.; Takeya, J.; Takimiya, K. Linear- and Angular-Shaped Naphthodithiophenes: Selective Synthesis, Properties, and Application to Organic Field-Effect Transistors. *J. Am. Chem. Soc.* **2011**, *133*, 5024−5035.
(16) Jang, J.; Nam, S.; Im, K.; Hur, J.; Cha, S. N.; Kim, J.; Son, H. B.; Suh, H.; Loth, M. A.; Anthony, J. E.; et al. Highly Crystalline Soluble Acene Crystal Arrays for Organic Transistors: Mechanism of Crystal Growth During Dip-Coating. *Adv. Funct. Mater.* **2012**, *22*, 1005−1014.
(17) Gundlach, D. J.; Lin, Y. Y.; Jackson, T. N.; Nelson, S. F.; Schlom, D. G. Pentacene Organic Thin-Film Transistors-Molecular Ordering and Mobility. *IEEE Electron Device Lett.* **1997**, *18*, 87−89.
(18) Yim, S.; Jones, T. S. Anomalous scaling behavior and surface roughening in molecular thin-film deposition. *Phys. Rev. B: Condens. Matter Mater. Phys.* **2006**, *73*, 161305.
(19) Kelley, T. W.; Frisbie, C. D. Gate Voltage Dependent Resistance of a Single Organic Semiconductor Grain Boundary. *J. Phys. Chem. B* **2001**, *105*, 4538−4540.
(20) Yang, J.; Yan, D. Weak epitaxy growth of organic semiconductor thin films. *Chem. Soc. Rev.* **2009**, *38*, 2634−2645.
(21) Wen, Y.; Liu, Y.; Guo, Y.; Yu, G.; Hu, W. Experimental Techniques for the Fabrication and Characterization of Organic Thin Films for Field-Effect Transistors. *Chem. Rev.* **2011**, *111*, 3358−3406.
(22) Hörmann, U.; Lorch, C.; Hinderhofer, A.; Gerlach, A.; Gruber, M.; Kraus, J.; Sykora, B.; Grob, S.; Linderl, T.; Wilke, A.; et al. V_{OC} from a Morphology Point of View: The Influence of Molecular Orientation on the Open Circuit Voltage of Organic Planar Heterojunction Solar Cells. *J. Phys. Chem. C* **2014**, *118*, 26462−26470.
(23) Kraus, M.; Richler, S.; Opitz, A.; Brütting, W.; Haas, S.; Hasegawa, T.; Hinderhofer, A.; Schreiber, F. High-mobility copper-phthalocyanine field-effect transistors with tetratetracontane passivation layer and organic metal contacts. *J. Appl. Phys.* **2010**, *107*, 094503−6.
(24) Klopotek, M.; Hansen-Goos, H.; Dixit, M.; Schilling, T.; Schreiber, F.; Oettel, M. Monolayers of hard rods on planar substrates. II. *J. Chem. Phys.* **2017**, *146*, 084903.
(25) Liscio, F.; Albonetti, C.; Broch, K.; Shehu, A.; Quiroga, S. D.; Ferlauto, L.; Frank, C.; Kowarik, S.; Nervo, R.; Gerlach, A.; et al. Molecular Reorganization in Organic Field-Effect Transistors and Its Effect on Two-Dimensional Charge Transport Pathways. *ACS Nano* **2013**, *7*, 1257−1264.
(26) Heinemeyer, U.; Broch, K.; Hinderhofer, A.; Kytka, M.; Scholz, R.; Gerlach, A.; Schreiber, F. Real-Time Changes in the Optical Spectrum of Organic Semiconducting Films and Their Thickness Regimes During Growth. *Phys. Rev. Lett.* **2010**, *104*, 257401.
(27) Lorch, C.; Banerjee, R.; Frank, C.; Dieterle, J.; Hinderhofer, A.; Gerlach, A.; Schreiber, F. Growth of competing crystal phases of α-sexithiophene studied by real-time X-ray scattering. *J. Phys. Chem. C* **2015**, *119*, 819−825.
(28) Anthony, J. E. Functionalized Acenes and Heteroacenes for Organic Electronics. *Chem. Rev.* **2006**, *106*, 5028−5048.
(29) Laquindanum, J. G.; Katz, H. E.; Lovinger, A. J. Synthesis, Morphology, and Field-Effect Mobility of Anthradithiophenes. *J. Am. Chem. Soc.* **1998**, *120*, 664−672.
(30) Payne, M. M.; Parkin, S. R.; Anthony, J. E.; Kuo, C.-C.; Jackson, T. N. Organic Field-Effect Transistors from Solution-Deposited Functionalized Acenes with Mobilities as High as 1 cm^2 /Vs. *J. Am. Chem. Soc.* **2005**, *127*, 4986−4987.
(31) Jurchescu, O. D.; Subramanian, S.; Kline, R. J.; Hudson, S. D.; Anthony, J. E.; Jackson, T. N.; Gundlach, D. J. Organic Single-Crystal Field-Effect Transistors of a Soluble Anthradithiophene. *Chem. Mater.* **2008**, *20*, 6733−6737.
(32) Chen, M.-C.; Kim, C.; Chen, S.-Y.; Chiang, Y.-J.; Chung, M.-C.; Facchetti, A.; Marks, T. J. Functionalized anthradithiophenes for organic field-effect transistors. *J. Mater. Chem.* **2008**, *18*, 1029−1036.
(33) Li, Z.; Lim, Y.-F.; Kim, J. B.; Parkin, S. R.; Loo, Y.-L.; Malliaras, G. G.; Anthony, J. E. Isomerically pure electron-deficient anthradithiophenes and their acceptor performance in polymer solar cells. *Chem. Commun.* **2011**, *47*, 7617.
(34) Reichenbächer, K.; Süss, H. I.; Hulliger, J. Fluorine in crystal engineering - "the little atom that could. *Chem. Soc. Rev.* **2005**, *34*, 22−30.
(35) Subramanian, S.; Park, S. K.; Parkin, S. R.; Podzorov, V.; Jackson, T. N.; Anthony, J. E. Chromophore Fluorination Enhances Crystallization and Stability of Soluble Anthradithiophene Semiconductors. *J. Am. Chem. Soc.* **2008**, *130*, 2706−2707.
(36) Coates, G. W.; Dunn, A. R.; Henling, L. M.; Ziller, J. W.; Lobkovsky, E. B.; Grubbs, R. H. Phenyl-Perfluorophenyl Stacking

DOI: 10.1021/acs.jpcc.7b06558
J. Phys. Chem. C 2017, 121, 21011−21017

Interactions: Topochemical (2 + 2) Photodimerization and Photopolymerization of Olefinic Compounds. *J. Am. Chem. Soc.* **1998**, *120*, 3641−3649.
(37) Anthony, J. E. Organic electronics: Addressing challenges. *Nat. Mater.* **2014**, *13*, 773−775.
(38) Lim, J. A.; Lee, H. S.; Lee, W. H.; Cho, K. Control of the Morphology and Structural Development of Solution-Processed Functionalized Acenes for High-Performance Organic Transistors. *Adv. Funct. Mater.* **2009**, *19*, 1515−1525.
(39) Diemer, P. J.; Hayes, J.; Welchman, E.; Hallani, R.; Pookpanratana, S. J.; Hacker, C. A.; Richter, C. A.; Anthony, J. E.; Thonhauser, T.; Jurchescu, O. D. The Influence of Isomer Purity on Trap States and Performance of Organic Thin-Film Transistors. *Adv. Electron. Mater.* **2017**, *3*, 1600294.
(40) Dürr, A. C.; Schreiber, F.; Ritley, K. A.; Kruppa, V.; Krug, J.; Dosch, H.; Struth, B. Rapid Roughening in Thin Film Growth of an Organic Semiconductor (Diindenoperylene). *Phys. Rev. Lett.* **2003**, *90*, 016104.
(41) Stadlober, B.; Haas, U.; Maresch, H.; Haase, A. Growth model of pentacene on inorganic and organic dielectrics based on scaling and rate-equation theory. *Phys. Rev. B: Condens. Matter Mater. Phys.* **2006**, *74*, 165302.
(42) Yang, J.; Yim, S.; Jones, T. S. Molecular-Orientation-Induced Rapid Roughening and Morphology Transition in Organic Semiconductor Thin-Film Growth. *Sci. Rep.* **2015**, *5*, 9441.
(43) Family, F. Dynamic scaling and phase transitions in interface growth. *Phys. A* **1990**, *168*, 561−580.
(44) Krug, J. Origins of scale invariance in growth processes. *Adv. Phys.* **1997**, *46*, 139−282.
(45) Krim, J.; Palasantzas, G. Experimental Observations of Self-Affine Scaling and Kinetic Roughening at Sub-Micron Lengthscales. *Int. J. Mod. Phys. B* **1995**, *9*, 599.
(46) Barabasi, A.-L.; Stanley, H. E. *Fractal Concepts in Surface Growth*; Columbia University Press: New York, 1995.
(47) Witte, G.; Wöll, C. Growth of aromatic molecules on solid substrates for applications in organic electronics. *J. Mater. Res.* **2004**, *19*, 1889−1916.
(48) Schreiber, F. Organic molecular beam deposition: Growth studies beyond the first monolayer. *phys. stat. sol. (a)* **2004**, *201*, 1037−1054.
(49) Hinderhofer, A.; Schreiber, F. Organic-organic heterostructures: Concepts and applications. *ChemPhysChem* **2012**, *13*, 628−643.
(50) Resel, R.; Bainschab, M.; Pichler, A.; Dingemans, T.; Simbrunner, C.; Stangl, J.; Salzmann, I. Multiple scattering in grazing-incidence X-ray diffraction: impact on lattice-constant determination in thin films. *J. Synchrotron Radiat.* **2016**, *23*, 729−734.
(51) von Helden, L.; Breuer, T.; Witte, G. Anisotropic thermal expansion in pentacene and perfluoropentacene: Effects of molecular packing motif and fixation at the interface. *Appl. Phys. Lett.* **2017**, *110*, 141904.
(52) Jones, A. O. F.; Chattopadhyay, B.; Geerts, Y. H.; Resel, R. Substrate-Induced and Thin-Film Phases: Polymorphism of Organic Materials on Surfaces. *Adv. Funct. Mater.* **2016**, *26*, 2233−2255.
(53) Yong, C. K.; Musser, A. J.; Bayliss, S. L.; Lukman, S.; Tamura, H.; Bubnova, O.; Hallani, R. K.; Meneau, A.; Resel, R.; Maruyama, M.; et al. The entangled triplet pair state in acene and heteroacene materials. *Nat. Commun.* **2017**, *8*, 15953.
(54) Michely, T.; Krug, J. *Islands, Mounds, and Atoms. Patterns and Processes in Crystal Growth Far from Equilibrium*; Springer: Berlin, 2004.
(55) Hlawacek, G.; Puschnig, P.; Frank, P.; Winkler, A.; Ambrosch-Draxl, C.; Teichert, C. Characterization of Step-Edge Barriers in Organic Thin-Film Growth. *Science* **2008**, *321*, 108−111.
(56) Gredig, T.; Silverstein, E. A.; Byrne, M. P. Height-Height Correlation Function to Determine Grain Size in Iron Phthalocyanine Thin Films. *J. Phys.: Conf. Ser.* **2013**, *417*, 012069.
(57) Zhang, X.; Barrena, E.; de Oteyza, D.; Dosch, H. Transition from layer-by-layer to rapid roughening in the growth of DIP on SiO_2. *Surf. Sci.* **2007**, *601*, 2420−2425.
(58) Zorba, S.; Shapir, Y.; Gao, Y. Fractal-mound growth of pentacene thin films. *Phys. Rev. B: Condens. Matter Mater. Phys.* **2006**, *74*, 245410.
(59) Kim, J.; Lim, N.; Park, C. R.; Yim, S. Growth dynamics of ZnPc and TiOPc thin films: Effect of crystallinity on anomalous scaling behavior. *Surf. Sci.* **2010**, *604*, 1143−1147.
(60) Kowarik, S.; Gerlach, A.; Sellner, S.; Schreiber, F.; Cavalcanti, L.; Konovalov, O. Real-time observation of structural and orientational transitions during growth of organic thin films. *Phys. Rev. Lett.* **2006**, *96*, 125504.
(61) Davydov, A. S. The theory of molecular excitons. *Sov. Phys. Usp.* **1964**, *7*, 145−178.
(62) Bortchagovsky, E. Ellipsometric method for investigation of the optical anisotropy of thin films: theory and calculations. *Thin Solid Films* **1997**, *307*, 192.
(63) Hinderhofer, A.; Heinemeyer, U.; Gerlach, A.; Kowarik, S.; Jacobs, R. M. J.; Sakamoto, Y.; Suzuki, T.; Schreiber, F. Optical properties of pentacene and perfluoropentacene thin films. *J. Chem. Phys.* **2007**, *127*, 194705.
(64) Hallani, R. K.; Thorley, K. J.; Mei, Y.; Parkin, S. R.; Jurchescu, O. D.; Anthony, J. E. Structural and Electronic Properties of Crystalline, Isomerically Pure Anthradithiophene Derivatives. *Adv. Funct. Mater.* **2016**, *26*, 2341−2348.

DOI: 10.1021/acs.jpcc.7b06558
J. Phys. Chem. C 2017, 121, 21011−21017